Marked Differences in Local Bone Remodeling Based on Marrow Stimulation Technique in a Large Animal

Hannah M Zlotnick, BS[1,2,3]
Ryan C Locke, PhD[1,3]
Brendan D Stoeckl, MSE[1,2,3]
Jay M Patel, PhD[1,3]
Sachin Gupta, MD[1,3]
Kevin D Browne, BA[4]
Jason Koh, MD, MBA[5]
James L Carey, MD, MPH[1,3]
Robert L Mauck, PhD[1,2,3]

[1]Dept. of Orthopaedic Surgery, University of Pennsylvania, Philadelphia, PA

[2]Dept. of Bioengineering, University of Pennsylvania, Philadelphia, PA

[3]Translational Musculoskeletal Research Center, Philadelphia VA Medical Center, Philadelphia, PA

[4]Center for Neurotrauma, Neurodegeneration, and Restoration, Philadelphia VA Medical Center, Philadelphia, PA

[5]Orthopaedic & Spine Institute, NorthShore University Health System, Evanston, IL

Introduction

Marrow stimulation is commonly performed to promote cell-mediated cartilage repair. Traditionally, a conical-tipped awl is used to perforate the underlying subchondral bone to enable the upward migration of marrow cells. However, awl-based microfracture results in irregular holes, inconsistent marrow effusion, and compacted bone[1]. In animal models, microfracture has also been shown to cause significant bone resorption[2], confounding the translation of augmented microfracture strategies. However, recent nanofracture approaches show promise[3]. In an effort to better understand the bony changes that occur post-microfracture, and improve upon the clinical gold standard of cartilage repair, we compared awl-based microfracture (Mfx) to other techniques—subchondral drilling (K-wire), and needle puncture (small SmartShot, large SmartShot)[4]—in a large animal cartilage defect repair model. We hypothesized that needle puncture would reduce bone resorption, and stimulate local bone formation at the puncture site, as assessed 4-weeks post-surgery.

Methods

Surgical Model

Six 1-year old castrated male Yucatan minipigs were used for this study. Six unilateral full thickness chondral defects (5 mm diameter) were created in the trochlear groove of the right hindlimb of each animal (Figure 1). Treatment conditions (1: empty defect, 2: Mfx (1.2 mm diameter, 2 mm depth, 3 holes), 3: K-wire drilling (1.25 mm diameter, 6 mm depth, 3 holes), 4: large SmartShot (1.2 mm diameter, 6 mm depth, 2 holes), 5: small SmartShot (0.9 mm diameter, 6 mm depth, 3 holes)) were randomized to defect location (n = 6-8 defects/treatment). Healthy cartilage, distal to the defects was used as a control for each animal. In conjunction with the knee procedure, an indwelling central venous catheter was implanted to facilitate fluorochrome labeling (xylenol orange (90 mg/kg) at the time of surgery and calcein (15 mg/kg) 2 weeks post-surgery). All animals were euthanized 4 weeks post-surgery.

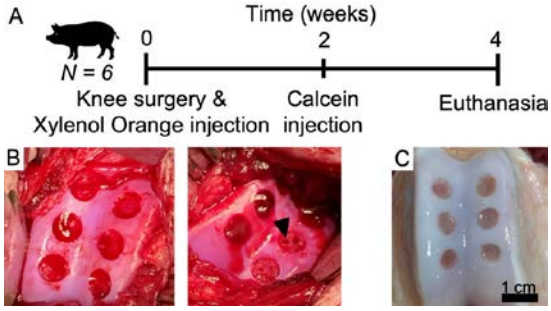

Figure 1. Study outline and macroscopic photos. **(A)** Study outline. **(B)** Six full thickness chondral defects in the trochlea, and treatment holes (arrowhead). **(C)** Gross view of cartilage healing at 4 weeks.

Micro-Computed Tomography & Analysis

Samples were scanned using a high resolution μCT (4.4 μm voxel size, SCANCO μCT50). 2D images were captured at the midplane of each sample, and FIJI was used to quantify the bone resorption area. Three blinded reviewers separately analyzed the images.

Mineralized Cryohistology & Analysis

All samples were formalin-fixed, infiltrated with a sucrose-polyvinylpyrrolidone solution, embedded, sectioned undecalcified with cryofilm, and imaged. After imaging fluorochrome labels, slides were stained for tartrate resistant acid phosphatase (TRAP), and imaged again[5].

Statistics

Figure 2: One-way ANOVA with Tukey's post-hoc test. Figure 3: Mann-Whitney test. Significance $p < 0.05$. Data shown: mean ± std dev.

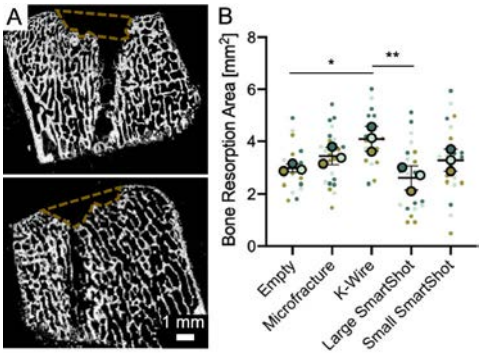

Figure 2. Bone resorption area decreases with SmartShot (needle puncture) device. **(A)** Representative μCT K-wire (top) and large SmartShot (bottom) images with quantified regions outlined. **(B)** Quantification of bone resorption area (n = 6-8 samples/treatment). Colors represent 3 separate blinded reviewers. ** $p < 0.01$, * $p < 0.05$.

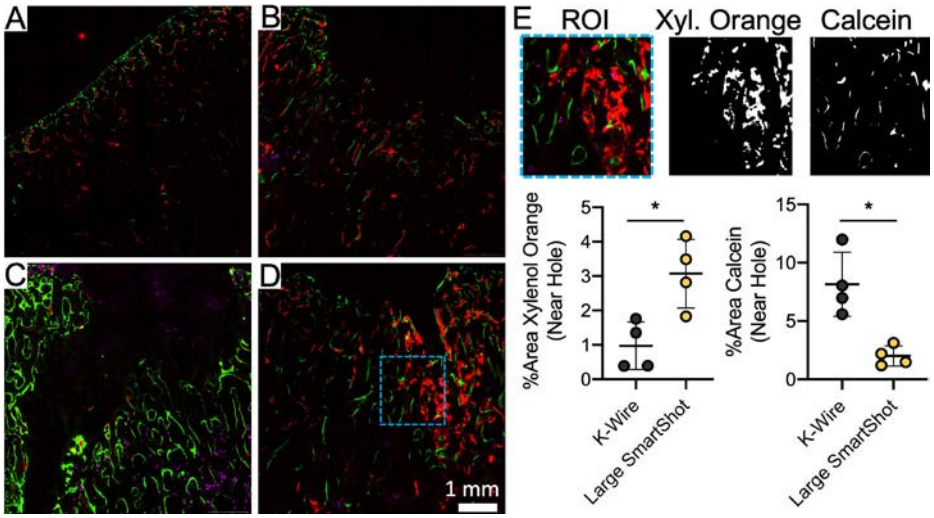

Figure 3. Dynamic bone remodeling in minipigs post-marrow stimulation. **(A-D)** Fluorochrome mineral labels (Xylenol Orange—red, Calcein—green) and tartrate resistant acid phosphatase staining (purple; osteoclasts). Images shown for intact cartilage, microfracture, K-wire, and large SmartShot, respectively. **(E)** Image analysis pipeline and quantification of the %Area of each mineral label proximal to the marrow stimulation hole (1.5 mm x 1.5 mm area). * $p < 0.05$. $n = 4$ defects/treatment quantified.

Results

While macroscopically the cartilage repair tissue looked similar across treatments at the 4-week sacrifice (Figure 1C), the subchondral bone showed marked differences. Defects treated with the K-wire underwent significant bone resorption in comparison to the empty (untreated) defects ($p < 0.01$), and defects treated with the large SmartShot ($p < 0.05$) (Figure 2). μCT images showed bony bridging/nascent bone formation across many of the SmartShot holes. In agreement with the bone resorption data, more osteoclasts (purple TRAP stain) were observed in the K-wire treated defects (Figure 3). Additionally, there was significantly less xylenol orange (1st injected mineral label) incorporation near K-wire holes, in comparison to SmartShot holes ($p < 0.05$). However, there was increased calcein (2nd injected mineral label) incorporation near the K-wire holes, suggesting a delayed subchondral remodeling in these defects.

Discussion

The health and strength of the subchondral bone likely plays a role in the downstream success or failure of a cartilage repair strategy. In this large animal study, drilling had the most deleterious impact on the underlying bone. Both μCT and bone fluorochrome labeling support the use of a more controlled, consistent needle puncture device for marrow stimulation. Further work will explore whether one or more of these bone metrics correlates with cartilage repair quality.

Significance

This is the first large animal study to utilize bone fluorochrome labeling to elucidate the dynamic bony changes that occur post-marrow stimulation. These results may directly guide clinical care and the development of improved micro/nanofracture devices.

References

1. Mithoefer K, McAdams T, Williams RJ, *et al*. Clinical efficacy of the microfracture technique for articular cartilage repair in the knee: an evidence-based systematic analysis (*Am J Sports Med*) 2009; 37(10): 2053-2063.

2. Gao L, Orth P, Muller-Brandt K, *et al*. Early loss of subchondral bone following microfracture is counteracted by bone marrow aspirate in a translational model of osteochondral repair (*Scientific Reports*) 2017; 7:45189.

3. Eldracher M, Orth P, Magali C, *et al*. Small subchondral drill holes improve marrow stimulation of articular cartilage defects (*Am J Sports Med*) 2014; 42(11): 2741-2750.

4. Koh J, Saladino J, Laughlin T, *et al*. Microfracture with Awls creates Significant Surface and Deep Damage in Standard Sized Defects compared to a Needle Marrow Access Device. (Orthopaedic Research Society Annual Meeting) 2020.

5. Dyment N, Jiang X, Chen L, *et al*. High-throughput, multi-image cryohistology of mineralized tissues (*J Vis*) 2016; (115): e54468.